OE Optical Engineering

RESEARCH PAPER

High-efficiency 2D grating design for the magneto-optical trap: enhancing intensity balance and reducing optical complexity

Elaheh Karooby,[a] **Jiazhen Li**,[a] **Amit Agrawal**,[b] **and Qing Gu**[a,c,*]

[a]North Carolina State University, Department of Electrical and Computer Engineering, Raleigh, North Carolina, United States

[b]University of Cambridge, Electrical Engineering Division, Department of Engineering, Cambridge, United Kingdom

[c]North Carolina State University, Department of Physics, Raleigh, North Carolina, United States

ABSTRACT. Integrated diffraction gratings offer a compact route to magneto-optical traps (MOTs) for atom cooling and trapping, thus preparing MOTs for future scalable quantum systems. Although segmented tri-gratings ensure axial radiation pressure balance, they are limited in optical trapping volume. Planar 2D gratings, though offer larger trapping regions, suffer from low diffraction efficiency and the resulting axial pressure imbalance, necessitating the use of a neutral density (ND) filter to achieve this balance. We present a numerically optimized 2D diffraction grating design that overcomes these limitations and satisfies the required optical conditions for laser cooling, namely, radiation pressure balance, specular reflection cancellation, and circular polarization handedness reversal upon diffraction, thus achieving an optical molasses—a necessary condition in MOT. Using rigorous coupled-wave analysis and a genetic algorithm, we design a grating for ^{87}Rb grating MOT (GMOT) that achieves a 24% first-order diffraction efficiency, of which 99.7% have the correct circular handedness. These properties enable efficient atom cooling without an ND filter when used with a flat-top beam inside the vacuum chamber. Our design simplifies optical alignment, reduces system footprint, and advances the integration of GMOTs into compact quantum devices.

 [DOI: 10.1117/1.OE.64.8.085106]

Keywords: magneto-optical trap; laser cooling and trapping; optical molasses; diffraction grating; genetic algorithm

Paper 20250529G received Jun. 25, 2025; revised Aug. 1, 2025; accepted Aug. 5, 2025; published Aug. 21, 2025.

1 Introduction

Magneto-optical traps (MOTs) are widely used to cool neutral atoms to sub-millikelvin temperatures[1] and trap them using a combination of laser light and magnetic fields. An MOT is a key tool for preparing ultracold atomic gases, which are crucial for exploring fundamental physics and technologies such as atomic clocks,[2] quantum computing and simulation,[3] and atom interferometry.[4]

An MOT typically uses six or four circularly polarized laser beams with appropriate handedness directed toward the trapping region. These lasers are red-detuned from the targeted atomic transition by a few natural linewidths (Γ). Thus, an atom experiences Doppler cooling as it moves toward each beam. Simultaneously, a spatial gradient magnetic field, created using a pair

*Address all correspondence to Qing Gu, qgu3@ncsu.edu

0091-3286/2025/$28.00

of anti-Helmholtz coils, provides a Zeeman shift to the atoms, pushing the atoms toward the center of the MOT. Together, a trapping region is formed near the zero gradient quadrupole magnetic field in the overlap region of multiple circularly polarized, red-detuned beams.

Traditionally, bulky MOT systems require complex configurations and intricate setups with six collimated laser beams and anti-Helmholtz coils. Shimizu's group experimentally showed that a three-dimensional (3D) MOT can be obtained using four collimated laser beams.[5,6] Over the past two decades, significant efforts have been made to miniaturize MOT systems using microfabricated atom chip traps.[7]

Two main types of miniature MOTs are pyramid MOT (PMOT)[8] and GMOT.[9–11] A PMOT uses a single circularly polarized input beam to form the optical trapping region, simplifying optical alignment by requiring only one laser beam. However, PMOTs are limited by the low atom capture capability ($\sim 10^7$ atoms)[12] and are thus not suitable for applications requiring high signal-to-noise ratios and atomic degeneracy, such as quantum information processing,[13] and high-resolution spectroscopy,[14] which require $>10^7$ atoms.

Although GMOTs operate on a similar principle to PMOTs, they overcome the low atom capture limitation by providing a larger overlap region, thanks to multiple diffraction orders from a large-area grating.[15] This enables GMOTs to trap 10^7 to 10^8 atoms.[15,16] Moreover, GMOTs minimize the intensity imbalance by allowing only a single pass of the trapping beam through the atomic cloud. It is, therefore, fair to say that GMOTs are superior to PMOTs for most applications.

Two types of planar grating chips have been employed in GMOTs: segmented tri-gratings that consist of three 1D gratings that are $2\pi/3$ rotated with respect to each other and extended toward the center of the chip[17–19] and 2D gratings.[20–22] For both grating geometries, chips with a 2×2 cm^2 area illuminated by a 2 cm diameter laser beam can provide optical overlap volumes of ~ 1 cm^3, significantly larger than the 0.01 cm^3 overlap volume of PMOTs.[15] The molasses works well for the segmented tri-grating chip because the three first-order diffractions, one from each segment, satisfy the condition for balanced optical intensity. However, the segmented tri-grating offers a smaller optical overlap volume than a 2D grating and, therefore, traps only 1/3 of the number of atoms.[15] In addition, there is a point of symmetry in the segmented tri-gratings' overlap volume, requiring precise alignment of the incident beam to the trapping point.[23] By contrast, the 2D grating has a larger overlap volume and does not require precise alignment as the grating profile is uniform across the entire chip surface. However, 2D gratings' low diffraction efficiency prevents them from meeting the required balanced optical intensity along the vertical axis, necessitating the use of an ND filter to achieve this balance.[20] Therefore, most state-of-the-art GMOTs use segmented tri-grating instead of a 2D grating to avoid optical complexity. Reference 24 optimized and fabricated a four-segment grating for GMOTs to set the targeted first-order diffraction efficiency to 25%, and Ref. 25 proposed a grating design methodology and applied it to segmented tri-gratings. Therefore, it is important to design high-efficiency 2D gratings for compact GMOTs that simultaneously satisfy the requirement of optical intensity balance along the vertical axis, allow easy alignment, and can trap a large number of atoms.

Previous studies have clearly identified the necessary optical conditions for efficient Doppler cooling and trapping, including optical intensity (radiation pressure) balance and circular polarization handedness reversal upon diffraction.[8,9,11]

In this work, we design and optimize a 2D dielectric diffraction grating with a metal back reflector that operates at 780 nm for ^{87}Rb GMOTs. The 2D grating can simultaneously support high first-order diffraction efficiencies, reflected order (specular reflection) cancellation, and high fidelity in maintaining the correct circular polarization handedness upon diffraction. At a normal incident wavelength of 780 nm, the grating achieves a diffraction efficiency of 24% for each of the $(\pm 1, 0)$ and $(0, \pm 1)$ diffraction orders, with 99.7% of the diffracted beams with the correct circular handedness. This design can enhance the performance of GMOTs employing 2D gratings by improving the axial radiation pressure balance and providing a high degree of circular polarization. Furthermore, we examine the gratings' manufacturing tolerance, demonstrating the robustness of our design to fabrication imperfections. We believe this work significantly improves over previously reported 2D gratings for GMOTs, paving the way for next-generation chip-scale MOTs requiring larger atom numbers. A preliminary version of this work, accepted for presentation at SPIE Optics + Photonics 2025, is available as Ref. 26.

2 Design and Optimization of the 2D Grating Atom Chip

Figure 1(a) illustrates the GMOT configuration, where a 2D grating diffracts a normally incident circularly polarized beam into four beams of first-order diffraction [Fig. 1(b)], forming a five-beam arrangement. The atom cloud can be trapped in the overlap region between the incident beam and the diffracted beams, positioned near the zero of the quadrupole magnetic field. When a laser beam is normally incident on the 2D grating, the diffraction angle θ—measured from the normal to the grating surface—for each order (m, n) is determined by the grating period Λ (considering $\Lambda_x = \Lambda_y = \Lambda$) relative to the incident wavelength λ, according to the Bragg condition

$$\Lambda \operatorname{Sin}\theta = \sqrt{m^2 + n^2}\lambda. \tag{1}$$

When Λ is restricted to the range $\lambda < \Lambda < \sqrt{2}\lambda$, the optical power is primarily distributed among the (0, 0), $(0, \pm 1)$, and $(\pm 1, 0)$ diffraction orders, whereas higher diffraction orders appear as evanescent waves on the grating, thus vanishing in the far field. For an incident wavelength of 780 nm, corresponding to the D2 transition (5S1/2 to 5P3/2) of ^{87}Rb, we design the grating period $\Lambda = 1080$ nm, resulting in a diffraction angle of $\theta = 46.24$ deg, which has experimentally shown to be appropriate for the GMOT.[15] Although the optimal diffraction angle θ for GMOTs cannot be analytically determined, it must meet a few specific requirements. First, θ must be greater than 30 deg for 1D gratings, and greater than 45 deg for 2D gratings, to avoid high diffraction orders. Second, a small θ leads to low radial trapping forces and reduces cooling and trapping efficiency.[8] Conversely, a very large θ significantly limits the trapping volume V, formed by the intersection of the incident and diffracted beams, thereby reducing the number of trapped atoms, $N_{\text{atoms}} \propto V^{1.2}$ according to an approximate scaling law[27]. The volume of the trapping region formed by the diffracted beams of a 2D grating with side length a, illuminated by a laser beam of diameter $2a$, can be approximated as the volume of a square pyramid with height $h (V = (1/3)a^2 h)$, where h is determined by θ.[15]

In an ideal GMOT, to achieve the balanced optical molasses condition, the optical forces acting on the atoms should sum to 0, both radially and vertically, at the center of the quadrupole magnetic field. This balance can be achieved by carefully designing the intensity and polarization of the input and diffracted light. Thanks to the symmetry of the 2D grating, radial optical balance is ensured, and the largest overlap volume is achieved when the incident beam is centered to illuminate the largest possible area of the grating. However, the axial balance is nontrivial because GMOTs spatially compress the incident beam upon diffraction, increasing the beam intensity in each diffraction order.[8] For our GMOT configuration, the diffraction orders of the grating must ensure balanced intensity along the vertical axis while facilitating the reversal of the handedness—the direction of circular polarization relative to the propagation direction—of the incident circularly polarized beam.

For an incident beam of intensity I_i, the intensity of each first-order diffracted beam is $I_d = \eta_{(1,0)}(w_i/w_d)I_i = \eta_{(1,0)}(I_i/\cos\theta)$, where $\eta_{(1,0)}$ is the efficiency of each first-order diffracted

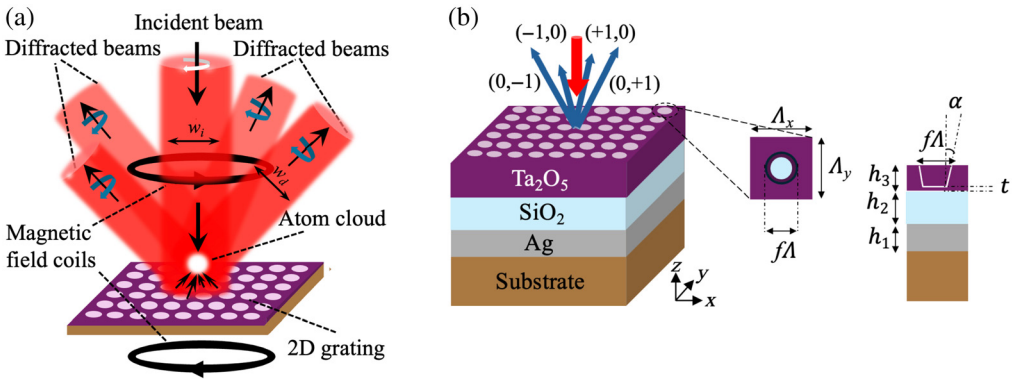

Fig. 1 Schematic of (a) atom cooling and trapping using a 2D diffraction grating atom chip. Black arrows point out the propagation direction of the incident and four first-order diffracted beams, with circular polarizations indicated by white and blue arrows, respectively. (b) The proposed 2D diffraction grating structure, with a top view and side view of a unit cell.

beam, and w_i and w_d are the beam waist of the incident and first-order diffracted beam, respectively, as illustrated in Fig. 1(a). For N first-order diffracted beams, the total upward intensity is $NI_d \cos\theta = N\eta_{(1,0)}I_i$ and the condition for vertical intensity balance require that $\eta_{(1,0)} = (1/N)$. Considering the net intensity incident on the grating chip as $I_i(1-\eta_{(0,0)})$, where $\eta_{(0,0)}$ represents the efficiency of the (0, 0) order, the vertical intensity balance can be quantified using a dimensionless parameter known as the radiation balance[21]

$$\eta_B = \frac{N\eta_{(1,0)}}{(1-\eta_{(0,0)})}, \tag{2}$$

with an ideal value of 1.

Another optical requirement of the grating concerns the polarization of the diffracted beams. The first-order diffracted beams must exhibit circular polarization with handedness opposite to that of the incident circularly polarized beam, aligning with the Zeeman effect in the atom's interaction with the magnetic field. By contrast, the reflected order must maintain the same handedness as the incident beam to prevent anti-trapping. Expressing the electric field vector of each first-order diffracted beam with S and P polarization components of intensities I_s and I_P, respectively, and a phase difference of φ_{SP}, we can write

$$\begin{pmatrix} \sqrt{I_s} \\ \sqrt{I_p}e^{i\varphi_{SP}} \end{pmatrix} = \sqrt{I_+}\exp(i\varphi_+)\begin{pmatrix} 1 \\ +i \end{pmatrix} + \sqrt{I_-}\exp(i\varphi_-)\begin{pmatrix} 1 \\ -i \end{pmatrix}. \tag{3}$$

Equation (3) can be rewritten in terms of the contrast of oppositely handed circular polarizations, which either trap or anti-trap the atoms (denoted by + or − subscripts, respectively), representing the degree of circular polarization

$$\xi_{SP} = \frac{I_+ - I_-}{I_+ + I_-} = \frac{2\sqrt{\frac{I_s}{I_p}}\sin\varphi_{SP}}{1+\frac{I_s}{I_p}}. \tag{4}$$

Ideally, $I_+ = 1$ and $I_- = 0$, resulting in $\xi_{SP} = 1$.

Illustrated in Fig. 1(b), the diffractive grating chip is based on a 2D square lattice of nanoholes within a tantalum pentoxide (Ta_2O_5)[28] layer of thickness h_3, which interfaces with a silicon dioxide (SiO_2) buffer layer of thickness h_2, deposited above a silver (Ag) film back reflector of thickness h_1. The buffer layer, with an optimized thickness h_2, primarily fine-tunes the optical path length, enabling phase adjustment of the incident light after it passes through the dielectric grating and reflects off the metal back reflector for optimal reflection. The material of the back reflector is silver (Ag) as it functions as an excellent reflector in the near-infrared regime and therefore can reflect the 780 nm incident light. Zerodur is selected as the substrate due to its low thermal expansion coefficient and high resistance to deformation under various temperatures.[29] At 780 nm, the refractive indices of Ta_2O_5, SiO_2, and Ag are 2.1,[30] 1.45,[31] and (0.0905 + i5.0617),[32] respectively. For the top Ta_2O_5 nanohole 2D grating, we consider a realistic scenario of the etched nanohole exhibiting a tapered sidewall with tilt angle α. To account for etching errors, we consider an unetched Ta_2O_5 layer of thickness t; namely, the nanoholes are of height $h_3 - t$. We use the GD-Calc open-source code[33] based on RCWA to design the 2D grating. All RCWA simulations are performed using an expansion basis of $2 \times 64 + 1$ plane waves. The conical frustum hole was discretized into 50 layers along the vertical direction for numerical modeling, and to approximate the cylindrical structure using block partitioning, the radius of the circular cross-section was discretized into 200 segments.

Although the multilayer 2D grating geometry itself is not unique, this study is distinguished by its specific design requirements for GMOTs. 2D gratings have been designed for various applications, typically optimized to maximize a particular diffraction order under a specific incident polarization, usually linear.

For the 2D grating studied here, high-efficiency first-order diffracted beams are essential for improving optical intensity balance along the vertical axis. By contrast, the reflected order must be suppressed, as its circular polarization handedness is different from the incident beam, which can cause anti-trapping. Therefore, we need to optimize the grating structure to simultaneously maximize the first-order diffraction efficiency and minimize the reflected order efficiency while

ensuring that the first-order diffracted beams exhibit a high degree of circular polarization with the correct handedness. The geometrical parameters of the 2D grating, including the fill factor f (the ratio of the hole diameter to the period), SiO_2 thickness h_2, Ta_2O_5 thickness h_3, tilt angle α, and the unetched Ta_2O_5 thin film thickness t, all influence the diffraction efficiency and the polarization. We design the grating period Λ and fill factor f along orthogonal directions in the xy plane to be equal, denoted as $\Lambda(\Lambda_x = \Lambda_y)$ and $f(f_x = f_y)$. This design choice $\Lambda_x = \Lambda_y$ ensures a spatially isotropic GMOT. Λ and the thickness of the silver film (h_1) are not included in the optimization process and are fixed at 1080 and 200 nm, respectively. As the grating exhibits high diffraction efficiencies for $h_1 \geq 180$ nm, we fixed $h_1 = 200$ nm to ensure strong performance and reduced the optimization time by excluding it from the optimization process.

We employ a genetic algorithm (GA) to optimize the parameters f, h_2, and h_3, first assuming straight sidewalls ($\alpha = 0$) and fully etched Ta_2O_5 nanoholes ($t = 0$ nm), where t denotes the thickness of any residual Ta_2O_5 layer remaining at the bottom of the nanoholes, due to imperfect control of etching height [Fig. 1(b)]; ideally, $t = 0$ nm, indicating complete etching through the nanoholes, with no residuals. In our design, we used MATLAB's genetic algorithm with 90 generations, a population size of 50, a function tolerance of 1×10^{-6}, and default settings for mutation, which provided a good balance between convergence reliability and computational time. The cost function (CF) is defined as CF = 0.5—$(\eta_{0,1} + \eta_{1,0})$, where $\eta_{0,1}$ and $\eta_{1,0}$ represent the diffraction efficiencies of the (0,1) and (1,0) diffraction orders for a circularly polarized incident beam. Due to the rotational symmetry of the 2D grating, the $(0, \pm 1)$ orders and the $(\pm 1, 0)$ orders always have the same diffraction efficiencies under a circularly polarized incident beam, we therefore only consider the (0,1) and (1,0) orders in the cost function. The purpose of this optimization is to minimize the CF, which corresponds to maximizing the diffraction efficiency of the first order while simultaneously ensuring that other figures of merit remain within our specified bounds ($\xi_{SP} \geq 98\%$ and $\eta_{(0,0)} \leq 0.6\%$) using a programmatic approach. Once the optimization algorithm finds the optimal set of geometrical parameters that minimizes the cost function, the code checks if the values ξ_{SP} and $\eta_{(0,0)}$ are within our specified bounds. If the condition is not met, the code penalizes the cost function and asks the algorithm to find an alternative set of optimized geometrical parameters. Once all three conditions are met, the algorithm stops, and $\eta_{(1,0)} = 24\%$ and $\xi_{SP} = 99.4\%$ are obtained for optimized parameters $f = 0.48$, $h_2 = 520$ nm, and $h_3 = 238$ nm, assuming $\alpha = 0$ deg, $t = 0$ nm. To the best of our knowledge, this represents the highest efficiency reported to date for 2D gratings that meet the optical requirements for GMOTs. Reference 21 proposed a 2D grating with a 180 nm gold (Au) reflection coating and reported a first-order diffraction efficiency of <20% and 15% for a 2D grating with a 100 nm Aluminum (Al) coating. Reference 15 measured a first-order diffraction efficiency of ~21% for an Au-coated grating. However, Au-coated gratings are not suitable for in-vacuum use as ^{87}Rb inside the vacuum system tends to chemically corrode the gold layer.

By substituting $\eta_{(1,0)} = 24\%$ and $\eta_{(0,0)} = 0.5\%$ in Eq. (2), a high radiation balance of $\eta_B = 96.6\%$ is obtained. The designed 2D grating, with its high-efficiency first-order beams, enhances the optical intensity balance along the vertical axis of GMOTs with 2D gratings. It can potentially reduce the temperature of the molasses without the need for an ND filter to compensate for the axial intensity imbalance due to low efficiency, if placed inside the vacuum chamber and illuminated by a flat-top beam. In previous studies, GMOTs utilizing low-efficiency 2D gratings required an ND filter to achieve the axial optical intensity balance.[20,21] If the incident beam has a Gaussian profile, as the atomic cloud position is raised above the grating surface, the contributing diffracted orders originate from progressively lower intensity regions of the Gaussian beam. This results in a vertical imbalance in radiation pressure and pushes the atomic cloud position downward relative to the center of the quadrupole magnetic field.[20] This leads to reduced atom number, increased molasses temperature, and degraded sub-Doppler cooling performance. Although a flat-top beam is ideal, using a Gaussian beam with a high-efficiency grating can still support efficient sub-Doppler cooling by raising the atomic cloud position to a location where optical forces are balanced.

Figure 2 illustrates the diffraction efficiencies of the first and the reflected order beams as a function of SiO_2 and Ta_2O_5 thicknesses, with a fill factor of 0.48 and straight sidewalls. The 2D grating under circularly polarized illumination achieves a first-order diffraction efficiency of greater than 22%, whereas the reflected order is lower than 0.10, shown in the region enclosed

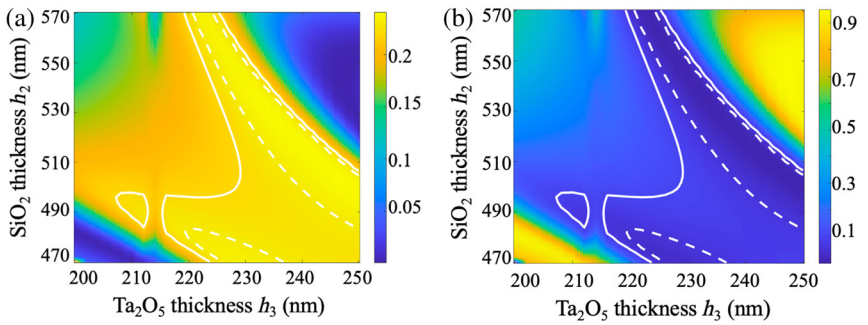

Fig. 2 Diffraction efficiency of (a) each first order and (b) reflected order of the grating as a function of SiO2 thickness $h2$ and Ta_2O_5 thickness $h3$, with $f = 0.48$ and $\alpha = 0$ deg.

by the solid contour. For a smaller SiO_2 thickness variation in the range of 504 to 528 nm and Ta_2O_5 thickness in the range of 232 to 242 nm, which are readily achievable with thin film deposition techniques, the dashed contours show regions of high diffraction efficiencies above 23%, where optimal performance occurs.

In GMOTs, it is essential that the 2D grating can reverse the handedness of the circularly polarized incident beam upon diffraction. Our optimized 2D grating can diffract the incident beam into four first orders, with $\xi_{SP} = 99.4\%$, resulting in a high proportion of circularly polarized light with the correct handedness, $I_+ = 99.7\%$, as calculated from Eq. (4). This high degree of circular polarization is more than adequate to create an efficient MOT and exceeds the values reported in previous studies of 2D gratings for GMOTs.[15,21] The high value of ξ_{SP} is primarily attributed to the phase difference between the S and P components φ_{SP} of the electric field vector of each first order, which is very close to $\pi/2$. Table 1 lists the diffraction efficiencies and polarization purities reported in this work and in previous studies on 2D gratings.

Figure 3 illustrates the effect of variations in the SiO_2 and Ta_2O_5 thicknesses, h_2 and h_3, respectively, on the parameter ξ_{SP} for the first and reflected order beams of the grating with a fill factor of 0.48 and straight sidewalls. For each first-order beam [Fig. 3(a)], a positive value of ξ_{SP} corresponds to the correctly handed circular light for MOT operation (with handedness opposite

Table 1 Diffraction efficiencies and polarization purities of several related works.

Reference	Diffraction efficiency ($\eta_{(1,0)}$)	Polarization purity (I_+)	Grating top layer material	Data type	Suitable for in-vacuum use
21	20%	98%	180 nm Au	Experimental	No
21	15%	99%	100 nm Al	Experimental	Yes
15	21%	—	100 nm Au	Experimental	No
This work	24%	99.7%	Ta_2O_5	Numerical	Yes

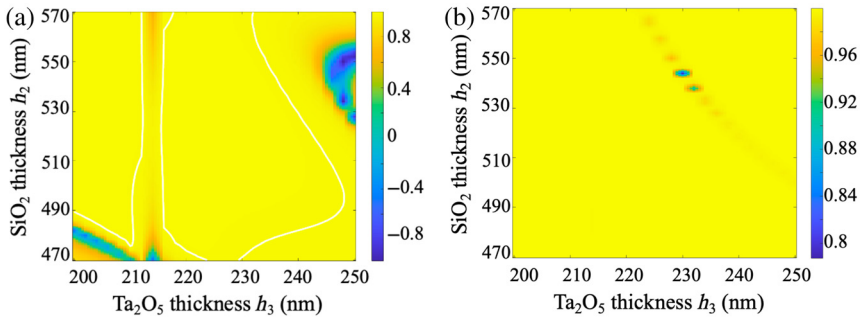

Fig. 3 Distribution of ξ_{SP} for (a) each first order and (b) reflected order of the grating as a function of SiO2 thickness $h2$ and Ta2O5 thickness $h3$, with $f = 0.48$, and $\alpha = 0$ deg. The solid contour outlines the region, where $\xi_{SP} > 99\%$.

to that of the incident beam), whereas a negative value of ξ_{SP} indicates the undesired handedness. The solid white contour surrounds the region where $\xi_{SP} > 99\%$, confirming that the optimized 2D grating shows a high fabrication tolerance to the thickness variation of the SiO_2 and Ta_2O_5. Figure 3(b) demonstrates the undesired circular polarization handedness of the reflected order (positive value of ξ_{SP}) as it must maintain the same handedness as the incident beam to prevent anti-trapping. For this reason, the efficiency of the reflected order is minimized during the optimization process, as shown in Fig. 2(b).

3 Robustness Analysis

The proposed 2D grating chip can be fabricated using either electron beam lithography or scanning beam interference lithography, followed by reactive ion etching (RIE).[34] Due to inevitable fabrication variations, including grating hole diameter variation that results in variation in the fill factor f, tapered sidewalls from RIE that results in a tilt angle α, and grating holes' height variation that results from unetched Ta_2O_5 thin film t, it is desirable that the grating performance metrics, such as the diffraction efficiency and fidelity in maintaining the correct polarization handedness upon diffraction, are tolerant to these fabrication variations. A reduction in the diffraction efficiency resulting from such imperfections can lead to higher molasses temperatures and less effective cooling. Similarly, lower polarization purity can weaken atom confinement and reduce the number of trapped atoms, thus decreasing the overall trapping efficiency.

Figure 4(a) shows the effect of unetched Ta_2O_5 thin film thickness t on the diffraction efficiency of the first and reflected orders, ξ_{SP}, and radiation balance η_B, whereas the other geometrical parameters are held at their optimal values ($f = 0.48$, $h_2 = 520$ nm, $h_3 = 238$ nm), assuming $\alpha = 0$ deg. For $t < 5$ nm, the diffraction efficiencies of the first orders exceed 23%, with $\xi_{SP} > 99.3\%$, resulting in $\eta_B > 96.5\%$. Therefore, our grating design shows an acceptable tolerance to the thickness variation of the unetched Ta_2O_5 thin film t. To model the residual layer in the RCWA simulations, a homogenous Ta_2O_5 layer was inserted between the buffer layer of thickness $h_2 = 520$ nm and the grating layer of thickness $h_3 = 238$ nm t. The height of the grating layer decreases as the height of the residual layer t increases.

In addition, the sidewall tilt angle reflects the fact that, during dry etching, the nanoholes deviate from a cylindrical shape to take on a frustum shape [Fig. 1(b)]. Figure 4(b) illustrates the dependence of the diffraction efficiencies, ξ_{SP} and η_B, on the grating sidewall tilt angle α, whereas the other geometrical parameters are held at their optimal values ($f = 0.48$, $h_2 = 520$ nm, $h_3 = 238$ nm, and $t = 0$ nm). For $\alpha < 15$ deg, the first-order diffraction efficiency is higher than 22%, with $\xi_{SP} > 95.5\%$, leading to $\eta_B > 96.5\%$. To model the sidewall tilt angle in RCWA simulations, we approximated the tapered nanohole profile by dividing the grating layer into 50 strata along the vertical direction. Each stratum was further partitioned into parallel stripes and then into circular blocks representing the air holes, with the radius discretized into 200 segments. The hole radius in each stratum was adjusted geometrically based on α, resulting in a gradual increase in the diameter with height, thus mimicking the sidewall tapering.

Figure 5 illustrates the diffraction efficiencies of the first and reflected orders as a function of the fill factor f and sidewall tilt angle α when the unetched Ta_2O_5 film thickness is $t = 0$ nm

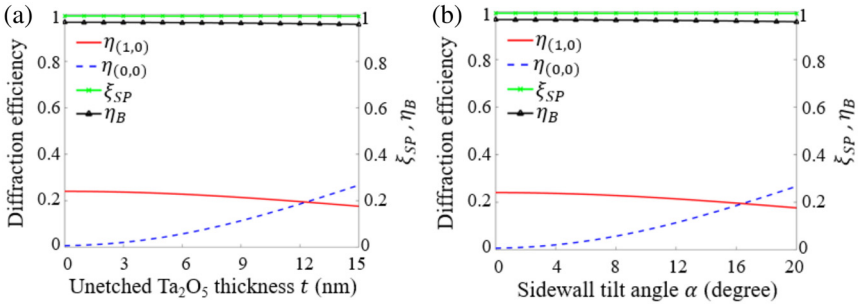

Fig. 4 Diffraction efficiency of the optimized grating, ξ_{SP}, and radiation balance η_B as a function of (a) unetched Ta2O5 thin film thickness t and (b) sidewall tilt angle α, under normal incidence of circularly polarized light.

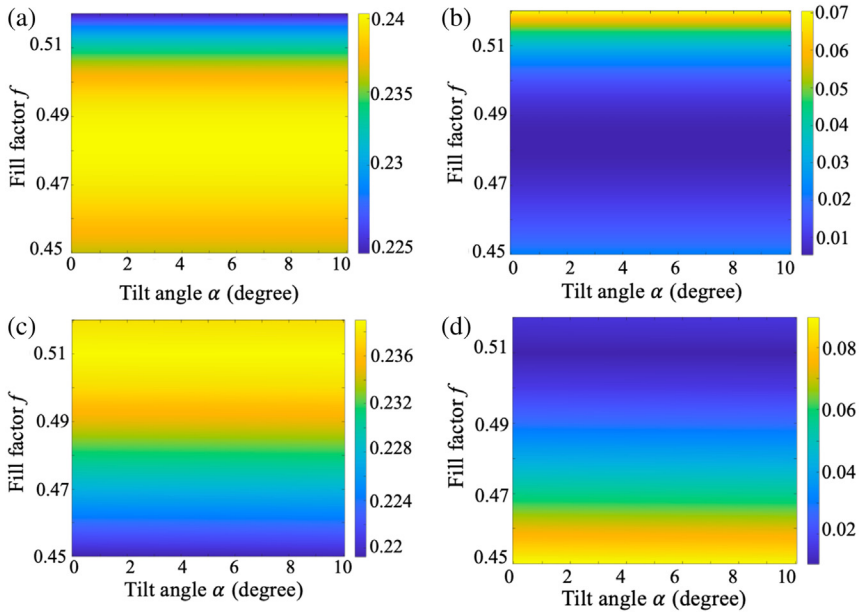

Fig. 5 Diffraction efficiency of (a), (c) each first order and (b), (d) reflected order of the grating as a function of fill factor f and sidewall tilt angle α, at (a), (b) $t = 0$ and (c), (d) $t = 5\ n$, with $h_2 = 520$ nm and $h_3 = 238$ nm.

[Figs. 5(a) and 5(b)] and $t = 5$ nm [Figs. 5(c) and 5(d)]. For $t = 0$ nm, a high first-order diffraction efficiency exceeding 24% is achieved with a fill factor of $0.473 - 0.489$ and a sidewall tilt angle of 0 to 10 deg, demonstrating that the optimized 2D grating exhibits a high tolerance to variations in both the fill factor and sidewall tilt angle. For $t = 5$ nm, the first-order diffraction efficiency at the fill factor $f = 0.48$ decreases from 24% of $t = 0$ nm to 23.1%. However, higher diffraction efficiencies are seen at larger fill factors, which is attributed to the unetched Ta_2O_5 film increasing the effective index of the grating structure. Consequently, a higher fill factor compensates for this increase in the effective index, leading to a higher diffraction efficiency.

Figure 6 illustrates the effect of variations in the fill factor f and sidewall tilt angle α on the parameter ξ_{SP} for the first and reflected orders when the unetched Ta_2O_5 film thickness is $t = 0$

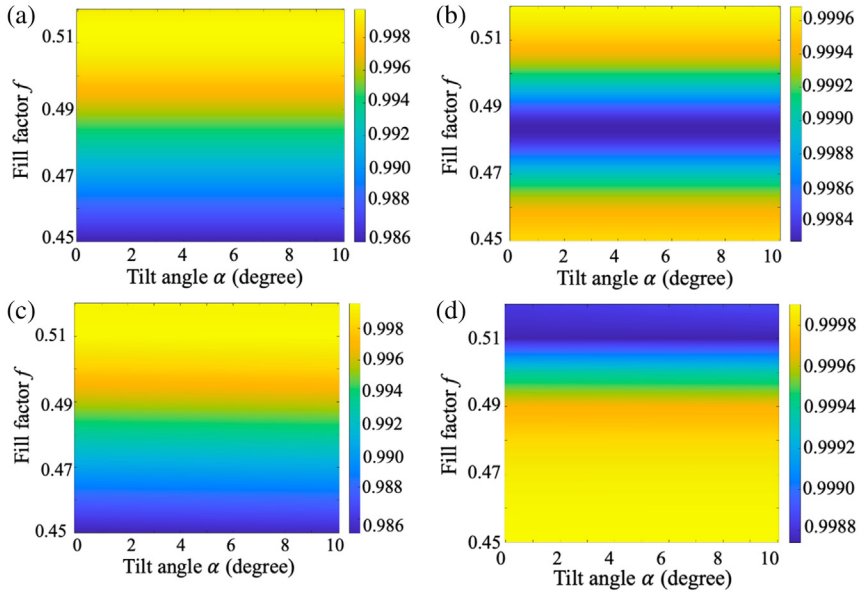

Fig. 6 Distribution of ξ_{SP} for (a), (c) each first order, (b), (d) reflected order of the grating as a function of fill factor f and sidewall tilt angle α, at (a), (b) $t = 0$ and (c), (d) $t = 5$ nm, with $h_2 = 520$ nm and $h_3 = 238$ nm.

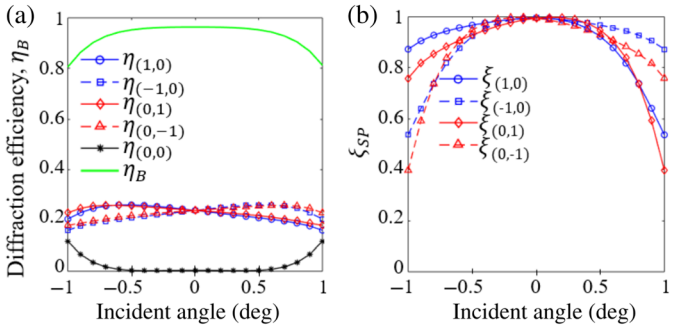

Fig. 7 (a) Diffraction efficiency of each first-order beam and the radiation balance η_B, and (b) degree of circular polarization ξ_{SP}, as a function of incident angle of the optimized grating.

[Figs. 6(a) and 6(b)] and $t = 5$ nm [Figs. 6(c) and 6(d)]. For the first orders [Figs. 6(a) and 6(c)], for both $t = 0$ nm and $t = 5$ nm, $\xi_{SP} > 98.6\%$ can be achieved with a fill factor in the range of 0.45 to 0.52 and a sidewall tilt angle of 0 to 10 deg, which demonstrates that the optimized 2D grating exhibits a high tolerance to variations in both the fill factor and sidewall tilt angle. Figures 6(b) and 6(d) demonstrate the undesired circular polarization handedness of the reflected order (positive value of ξ_{SP}); however, the efficiency of the reflected order beam is minimized during the optimization process [Figs. 5(b) and 5(d)].

To evaluate the robustness of the grating to angular misalignment, we analyzed the impact of the incident angle on the diffraction efficiency of each first-order beam, the radiation balance parameter η_B, and the degree of circular polarization ξ_{SP}. As shown in Fig. 7(a), the diffraction efficiencies of the $(0, \pm 1)$ orders change inversely with angle. A similar trend is observed for the $(\pm 1, 0)$ orders. Moreover, a small deviation from normal incidence breaks the balance of the first-order beams and increases the intensity of the undesired reflected order. Within an angular tolerance of $\sim \pm 0.7$ deg, the grating maintains high performance. Specifically, η_B remains above 92.66%, as shown in Fig. 7(a), and ξ_{SP} exceeds 81.65% for all first-order beams, as illustrated in Fig. 7(b).

We also investigated the use of titanium dioxide (TiO_2) as an alternative grating material, paired with either Zerodur or fused silica substrates. Although we were able to optimize the geometrical parameters of TiO_2 gratings to achieve high efficiencies, none simultaneously provided both high circular polarization purity and robust fabrication tolerance. Our optimized TiO_2 gratings either exhibited limited fabrication tolerance, for example, $\alpha < 2.6$ deg, or a low degree of circular polarization, such as $\xi_{SP} = 0.67$.

4 Conclusion

This work computationally investigates a 2D diffraction grating with high efficiency and strong circular polarization flipping properties for insertion in GMOTs. Simulation with RCWA and optimization with GA shows that the diffraction efficiency of each of the $(\pm 1, 0)$ and $(0, \pm 1)$ orders can reach as high as 24%, with 99.7% of the diffracted light exhibiting the correct circular polarization handedness ($I_+ = 99.7\%$), resulting in a high radiation balance greater than 96.6% along the vertical axis of GMOTs. The proposed grating offers significant advancement for GMOTs by eliminating the need for an ND filter to balance axial optical intensity, previously required in GMOTs with low-efficiency 2D gratings. When placed within the chamber and illuminated by a flat-top beam, it effectively reduces the molasses temperature without additional components.

Furthermore, our design has a high resilience to manufacturing variations, maintaining performance despite deviations in critical geometrical parameters such as sidewall tilt angle α, fill factor f, and unetched Ta_2O_5 thin film thickness t deviates from optimal values. Compared with existing 2D gratings and segmented tri-gratings, our proposed 2D grating represents a superior solution by simultaneously addressing multiple GMOT requirements of simplified alignment, large trapping volume for increased atom capture, and enhanced overall system compactness.

Disclosures

The authors declare that there are no financial interests, commercial affiliations, or other potential conflicts of interest that could have influenced the objectivity of this research or the writing of this paper.

Code and Data Availability

The data supporting the plots within this paper and other findings of this study are available from the corresponding author upon reasonable request.

Acknowledgments

This work was supported by the National Science Foundation (CAREER ECCS-2209871 and ExpandQISE-2329027). We thank Aidan Arnold of the University of Strathclyde for fruitful discussions.

References

1. E. L. Raab et al., "Trapping of neutral sodium atoms with radiation pressure," *Phys. Rev. Lett.* **59**(23), 2631–2634 (1987).
2. S. Jammi et al., "Alignment-free Sr MOT with integrated metasurfaces for a compact Sr optical clock," in *CLEO: Science and Innovations*, p. SW4O-2, Optica Publishing Group (2023).
3. C. J. Picken et al., "Entanglement of neutral-atom qubits with long ground-Rydberg coherence times," *Quantum Sci. Technol.* **4**(1), 015011 (2018).
4. X. Dong et al., "Study to improve the performance of interferometer with ultra-cold atoms," *Chin. Phys. B* **30**(1), 014210 (2021).
5. H. Takuma, K. Shimizu, and F. Shimizu, "Four-beam laser trap of neutral atoms," *Opt. Lett.* **16**(5), 339–341 (1991).
6. Z. Lin et al., "Laser cooling and trapping of LI," *Jpn. J. Appl. Phys.* **30**(7), 1324–1326 (1991).
7. Z. Tan et al., "Compact magneto-optical traps using planar optics," *Chin. Phys. B* **33**(9), 093701 (2024).
8. M. Vangeleyn et al., "Single-laser, one beam, tetrahedral magneto-optical trap," *Opt. Express* **17**(16), 13601–13608 (2009).
9. M. Vangeleyn et al., "Laser cooling with a single laser beam and a planar diffractor," *Opt. Lett.* **35**(20), 3453 (2010).
10. W. R. McGehee et al., "Magneto-optical trapping using planar optics," *New J. Phys.* **23**(1), 013021 (2021).
11. J. Lee et al., "Sub-Doppler cooling of neutral atoms in a grating magneto-optical trap," *J. Opt. Soc. Am. B* **30**(11), 2869 (2013).
12. J. A. Kim et al., "Single-beam atom trap in a pyramidal and conical hollow mirror," *Opt. Lett.* **21**(15), 1177–1179 (1996).
13. H. Weimer et al., "A Rydberg quantum simulator," *Nat. Phys.* **6**(5), 382–388 (2010).
14. T. Kisters et al., "High-resolution spectroscopy with laser-cooled and trapped calcium atoms," *Appl. Phys. B* **59**(2), 89–98 (1994).
15. C. C. Nshii et al., "A surface-patterned chip as a strong source of ultracold atoms for quantum technologies," *Nat. Nanotechnol.* **8**(5), 321–324 (2013).
16. E. Imhof et al., "Two-dimensional grating magneto-optical trap," *Phys. Rev. A* **96**(3), 033636 (2017).
17. J. P. Cotter et al., "Design and fabrication of diffractive atom chips for laser cooling and trapping," *Appl. Phys. B* **122**(6), 1–6 (2016).
18. J. Duan et al., "High diffraction efficiency grating atom chip for magneto-optical trap," *Opt. Commun.* **513**, 128087 (2022).
19. D. S. Barker et al., "Grating magneto-optical traps with complicated level structures," *New J. Phys.* **25**(10), 103046 (2023).
20. J. P. McGilligan et al., "Phase-space properties of magneto-optical traps utilising micro-fabricated gratings," *Opt. Express* **23**(7), 8948–8959 (2015).
21. J. P. McGilligan et al., "Diffraction-grating characterization for cold-atom experiments," *JOSA B* **33**(6), 1271–1277 (2016).
22. S. Deshpande et al., "Rapid design and fabrication of grating chips for magneto-optical trapping of atoms," in *CLEO*, Optica Publishing Group, p. JTh2A.6 (2023).
23. J. P. McGilligan et al., "Micro-fabricated components for cold atom sensors," *Rev. Sci. Instrum.* **93**(9), 91101 (2022).
24. S. Bondza et al., "Two-color grating magneto-optical trap for narrow-line laser cooling," *Phys. Rev. Appl.* **17**(4), 044002 (2022).
25. R. Calviac et al., "Grating design methodology for laser cooling," *JOSA B* **41**(7), 1533 (2024).

26. E. Karooby et al., "Design and optimization of a high-efficiency and robust 2D grating for the magneto-optical trap," *Proc. SPIE* 13582-3, in press (2025).
27. K. Lindquist, M. Stephens, and C. Wieman, "Experimental and theoretical study of the vapor-cell Zeeman optical trap," *Phys. Rev.* **46**, 4082 (1992).
28. C. Zhang et al., "Tantalum pentoxide: a new material platform for high-performance dielectric metasurface optics in the ultraviolet and visible region," *Light Sci. Appl.* **13**(1), 23 (2024).
29. I. Mitra, "ZERODUR: a glass-ceramic material enabling optical technologies [Invited]," *Opt. Mater. Express* **12**(9), 3563–3576 (2022).
30. T. J. Bright et al., "Infrared optical properties of amorphous and nanocrystalline Ta 2O5 thin films," *J. Appl. Phys.* **114**(8) (2013).
31. I. H. Malitson, "Interspecimen comparison of the refractive index of fused silica," *J. Opt. Soc. Am.* **55**(10), 1205–1209 (1965).
32. A. Ciesielski et al., "Controlling the optical parameters of self-assembled silver films with wetting layers and annealing," *Appl. Surf. Sci.* **421**, 349–356 (2017).
33. K. C. Johnson, "Grating diffraction calculator (GD-Calc ®) [Source Code]," 2022, https://www.mathworks.com/products/connections/product_detail/gd-calc.html (accessed 5 March 2025).
34. C. G. Chen et al., "Nanometer-accurate grating fabrication with scanning beam interference lithography," *Proc. SPIE* **4936**, 126–134 (2002).

Elaheh Karooby is a PhD candidate in the Department of Electrical and Computer Engineering at North Carolina State University. She received her BS degree from Karaj Azad University and her MS degree from K. N. Toosi University of Technology, both in electrical engineering. Her research focuses on the design and development of quantum photonic devices for scalable quantum technologies. She is a member of SPIE.

Jiazhen Li is a postdoctoral researcher in the Department of Electrical and Computer Engineering at North Carolina State University. She received her BS degree from Taiyuan Normal University and her PhD from South China Normal University, both in physics. Her research focuses on combining the atom trapping system with nanodevices, such as metasurfaces and gratings, and developing chip-scale atomic systems.

Amit Agrawal is an associate professor of optical engineering at the University of Cambridge and a fellow and director of studies at Trinity College. He received his MS and PhD degrees from the University of Utah, followed by a postdoc at NIST. He then joined Syracuse University as an assistant professor and served in staff scientist roles at NIST and the US Army Research Laboratory. At Cambridge, he works in the areas of quantum integrated photonics.

Qing Gu is an associate professor at North Carolina State University with a joint appointment between ECE and physics. She received her BS degree from the University of British Columbia, Canada, in 2008, and her PhD from the University of California, San Diego, in 2014. Her research activities include the experimental realization of semiconductor nanoscale light sources, optical metamaterials, and nanophotonic devices for quantum photonics. She is a member of SPIE.